RESEARCH ARTICLE

Society For Biomaterials

WILEY

Freeze casting of hydroxyapatite-titania composites for bone substitutes

Tony J. Yin[1] | Samantha K. Steyl[2,3] | Jerry Howard[4] | Krista Carlson[4] | Sujee Jeyapalina[2,3] | Steven E. Naleway[1]

[1]Department of Mechanical Engineering, University of Utah, Salt Lake City, Utah, USA

[2]Division of Plastic Surgery, Department of Surgery, University of Utah School of Medicine, Salt Lake City, Utah, USA

[3]Department of Biomedical Engineering, University of Utah, Salt Lake City, Utah, USA

[4]Department of Chemical and Materials Engineering, University of Nevada, Reno, Reno, Nevada, USA

Correspondence
Steven E. Naleway, Department of Mechanical Engineering, University of Utah, Salt Lake City, UT, USA.
Email: steven.naleway@mech.utah.edu

Abstract

Hydroxyapatite (HA) is commonly used as a bone substitute material, but it lacks mechanical strength when compared to native bone tissues. To improve the efficacy of HA as a bone substitute by improving the mechanical strength and cell growth attributes, porous composite scaffolds of HA and titania (HA-TiO$_2$) were fabricated through a freeze-casting process. Three different compositions by weight percent, 25–75 HA-TiO$_2$, 50–50 HA-TiO$_2$, and 75–25 HA-TiO$_2$, were custom-made for testing. After sintering at 1250°C, these composite scaffolds exhibited improved mechanical properties compared to porous HA scaffolds. Substrate mixing was observed, which helped reduce crystal size and introduced new phases such as β-TCP and CaTiO$_3$, which also led to improved mechanical properties. The composition of 50–50 HA-TiO$_2$ had the highest ultimate compressive strength of 3.12 ± 0.36 MPa and elastic modulus 63.29 ± 28.75 MPa. Human osteoblast cell proliferation assay also increased on all three different compositions when compared to porous HA at 14 days. These results highlight the potential of freeze casting composites for the fabrication of bone substitutes, which provide enhanced mechanical strength and biocompatibility while maintaining porosity.

KEYWORDS
material characterization, scaffold fabrication, titanium dioxide

1 | INTRODUCTION

With a rise in orthopedic and dental implant procedures, effective bone grafts are needed to support the growing demand.[1] While autografts remain the gold standard mainly for their osteoinductivity, complications still arise from limited donor availability.[2,3] Allografts and xenografts remain viable alternatives but lack osteoinductive properties as they must be sterilized to prevent immunogenic responses.[3] Synthetic alloplasts have therefore been developed thanks to research combining biocompatible materials with innovative fabrication processes providing bone-like scaffolds.[4,5] These alloplasts can thus be tailored to have specific pore structures and mechanical properties and can be made from a wide variety of materials.[6] These benefits have led to an increase in artificial bone substitutes in recent years.[7] As such, much of bone tissue engineering has examined different combinations of materials and structures to improve the state of the art of bone substitutes. Bone tissue engineering aims to create a scaffold capable of matching the extracellular matrix, providing adequate mechanical strength for load-bearing sites, material compatibility required for biological signaling, and porosity needed for neo-vascularization, supporting cell adhesion, proliferation, and differentiation.[4,8,9]

Current challenges for artificial bone substitutes stem from the limited number of biomaterials with both adequate mechanical strength and chemical composition capable of meeting clinical standards.[1] Common ceramics used to create bone substitutes include hydroxyapatite (HA, Ca$_{10}$(PO$_4$)$_6$(OH)$_2$) and other calcium phosphate ceramics like tricalcium phosphate due to their similarity to the mineral phase in bone and their affordance for resorption.[8–12] These materials currently appear in a variety of forms, such as cements,[13]

coatings,[14] and implant hardware.[15] However, calcium phosphate ceramics are intrinsically mechanically weak.[10,11] The low mechanical strengths and stiffnesses prevent their use in load-bearing bone regions.[16] Additionally, the necessity for porosity for oxygen, nutrient, and waste transportation further reduces the mechanical stability.[8–12]

Focus on ceramic–ceramic composites, or composites that consist of two or more different ceramic chemical compounds, has led to improving this mechanical stability through the inclusion of mechanically stronger compatible counterparts that also further assist in load-bearing bone regeneration.[17,18] Titania (TiO_2) is one such material. It is commonly used in conjunction with HA because TiO_2 acts as an intermediary between HA coatings and titanium implants, and it is also a known osteoconductive material.[19,20] This capability helps it perform a major role as the intermediate layer between titanium alloy implants and the calcium phosphate coatings.[14,21] TiO_2 also has a higher mechanical strength than HA and has been shown to improve mechanical strength without worsening biocompatibility when added to calcium phosphate ceramics.[22,23] Past investigations on these composites have also shown increases in fracture strength, toughness, and stiffness in comparison to only HA.[24,25] As stated, HA and TiO_2 are both biocompatible ceramics with suitable properties to be used as bone substitute.[8–10] These two ceramics have been studied because of their complementary properties. Both ceramics remain thermally stable up to 1250°C.[24,25] They also provide unique benefits not seen in the partner material, with HA providing greater osteoconductivity and TiO_2 providing greater mechanical strength.[8–10] To expand on the previous knowledge of porous bioceramic composites, HA-TiO_2 scaffolds were made through freeze casting and tested for the uniaxial mechanical properties and in vitro osteoblast adhesion properties. Notably, freeze casting has not been used for HA-TiO_2 composite fabrication before.

In this article, we have fabricated porous HA-TiO_2 composite scaffolds using the freeze-casting method.[9,26–28] This technique involves the mixture of an aqueous slurry of ceramic powders, polymeric binders, and a dispersant. The slurry is directionally frozen to generate ice crystals with the ceramic particles pushed into the gaps between the crystal growths. By freeze-drying the structure and subsequently sintering the ceramic green body, a negative of the ice crystals is formed, yielding a ceramic scaffold with an interconnected directional pore structure and mechanical stability. This porous structure was achieved across multiple combinations of HA and TiO_2, showing compatibility between the two materials in meeting physical and biological needs. Chemical, structural, mechanical, and in vitro characterizations showed that HA-TiO_2 freeze-cast composite scaffolds have great potential as future bone substitutes because of their strength and biocompatibility.

2 | MATERIALS AND METHODS

2.1 | Scaffold fabrication

Freeze-cast scaffolds were prepared by first making aqueous slurries with four different solid loadings of HA and TiO_2 (referred to herein as composite loadings) of 10 volume percent (vol%) (Table 1) and

TABLE 1 Composite loadings by volume percentage of HA and TiO_2 in initial slurries.

Name	HA	HT-25	HT-50	HT-75	npHA
vol% HA	100	75	50	25	100
vol% TiO_2	0	25	50	75	0

mixed with water. Four composite loadings were made with HA in 10, 7.5, 5, and 2.5 vol% and TiO_2 in 0, 2.5, 5, and 7.5 vol% compositions. Samples with these composite loadings are referred to as HA (100% HA, 0% TiO_2), HT-25 (75% HA, 25% TiO_2), HT-50 (50% HA, 50% TiO_2), and HT-75 (25% HA, 75% TiO_2), respectively based on percentage TiO_2 content. To maintain structural integrity before sintering, both 1 weight percent (wt%) polyvinyl alcohol of 88,000–97,000 g/mol (Alfa Aesar, Ward Hill, MA, USA) and 1 wt% polyethylene glycol of 10,000 g/mol (Alfa Aesar, Ward Hill, MA, USA) were added to each slurry as binders. Weight percents were relative to composite loadings. To maintain a homogenous mixture during mixing, 1 wt% Dynol 604 (Evonik Industries, Essen, Germany) was added as a dispersant.[29] Lastly, 5 vol% of 97% isopropyl alcohol (Sigma–Aldrich, St. Louis, MO, USA) was added to increase pore size.[30,31]

Slurries were prepared in 15 mL batches, which were used to fabricate one scaffold each. The solid loading, water, and additives were sealed in a 40 mL plastic bag and then ultrasonicated at 42 kHz for 24 min, creating a colloidal suspension. Ultrasonication has successfully proven effective in mixing slurries for freeze casting.[30,32–35] After sonication, slurries were freeze cast with a cooling rate of 10°C/min.[30] To remove the ice from the freeze-cast slurries, each slurry was freeze-dried at 0.03 mBar and −51°C for 96 h. The weak porous structure obtained after the freeze drying was sintered in air for 3 h at 1250°C at a ramp rate of 3°C/min. The resulting product was a porous, freeze-cast scaffold measuring approximately 14 mm in diameter and 20 mm in height. In total, 6 scaffolds were made for each composite loading, totaling 24 scaffolds.

For cell culture controls, 6 additional nonporous HA discs were fabricated by mixing 300 mg of the HA with 0.7 μL of sterile water.[30,36] This mixture was then inserted into a 10 mm diameter die on a hydraulic press and compacted at 20 kPa under vacuum for 2 min[36] before sintering with the same procedure as above.

2.2 | Experimental sample preparation

The freeze-cast scaffolds were cut into smaller sections for the testing.[30] Scaffolds were cut 5 mm from the bottom to avoid dense regions.[37] The top 5 mm of each scaffold was also cut to avoid surface defects and potentially be used for structural imaging of the interior surface. The remaining middle section was bisected into two discs of 5 mm in thickness to be used for either mechanical testing or cell culturing studies. Samples that were intended for compression testing were further prepared by cutting the disc into quarter circles 5 mm in height and 6 mm in radius. Also, powder samples for x-ray diffraction

—WILEY—

were collected from these crushed compression samples post-testing. Cell culture samples consisted of the porous freeze-cast scaffold discs, nonporous HA (npHA) discs 10 mm in diameter and 2 mm in height and cell-drop controls with cells added directly to a well-plate.

For imaging, all six top sections of the freeze-cast scaffold per composite loading were used. For compression testing, three discs from three randomly selected scaffolds were used. For cell culturing, one disc per scaffold was used per composite loading.

2.3 | Microstructural characterization

Images of scaffold microstructures perpendicular to the freezing direction were observed through scanning electron microscopy (SEM; FEI Quanta 600 FG, Hillsboro, OR, USA) with a 4 nm spot size and 20 kV accelerating voltage. These samples were initially coated with a 20-nm layer of gold–palladium prior to imaging. Images from three samples per composite loading were used for analysis. Five distinct regions of each SEM sample were imaged, with 15 images of each composite loading being used in total. Image-J and the DiameterJ plugin[38] were used to measure the total porosity, wall thickness, and equivalent pore diameter from the SEM images. The porosity was measured as the percentage area of pores relative to the whole imaged area ($n = 15$ per composite loading, 60 total). Because of the elliptical pore shape, equivalent pore diameters were evaluated based on the mathematical relation of the ellipse perimeter to area for the elliptical pores.[30] Eighty pores per image were measured, resulting in 1200 measurements per composite loading and 4800 measurements in total. Wall thickness was measured as the average width along the length of the walls ($n = 80$ measurements per SEM image, 1200 measurements per composite loading, 4800 total).

2.4 | Material characterization

Element analysis using energy-dispersive x-ray spectroscopy (EDX) was performed to observe the presence and interaction of HA and TiO_2 after sintering. The elements of calcium and titanium were specifically examined as they represented regions of HA and TiO_2, respectively. These elements were also mapped to imaged regions for qualitative analysis. The presence, location, and arrangement of calcium and titanium in the different composite loadings were noted using three images from different scaffolds per composite loading.

To identify any crystallographic and phase composition changes, powder x-ray diffraction (XRD) of the different composite loadings was performed using a SmartLab (Rigaku, Tokyo, Japan). Powder samples were prepared from crushed, freeze-cast scaffolds with scans performed over a range of 10–70° 2θ with a step size of 0.05° 2θ at 0.5° 2θ/min. Four scans were performed for each composite loading from a single scaffold, resulting in 16 total scans.

2.5 | Mechanical testing

Mechanical properties of the freeze-cast scaffolds were determined through uniaxial compression testing performed using an Instron Model 5967 load frame (Instron, Norwood, MA, USA) with a 30 kN load cell. Using samples from three scaffolds, compression tests ($n = 11$ per composite loading, 44 total) were performed at a constant 1 mm/min crosshead speed along the freezing direction. The ultimate compressive strength (UCS) and elastic modulus (E) were calculated from the peak stress value and the linear region of the stress–strain curve, respectively.

2.6 | *In vitro* cell culturing

All cell culturing was performed aseptically to prevent contamination. Human osteoblast (hOB) cells were obtained from American Type Culture Collection (ATCC, Manassas, VA, USA) and cultured in complete hOB media composed of Dulbecco's modified Eagle's medium (DMEM), 10 vol% fetal bovine serum, and 0.3 mg/mL Geneticin-418 antibiotic for 4 days at 34°C and 5% CO_2. Phosphate buffered saline ($1\times$ PBS) was used to wash the samples every time before moving samples or changing media. The hOB cells were from passage 9 to prevent issues with cell health and gene expression.

Procedures for hOB cell culturing were performed as previously reported in Reference 30. Cell culture samples were sterilized by autoclave, followed by seeding of 60,000 hOB cells in 200 μL of media per sample.[30,36] Additional cell-drop control samples consisting of cells seeded directly into a 12-well plate were used. Cells were incubated for 2 h to allow cell attachment to the samples.[30,36] After the cell attachment period, samples were submerged in 2 mL of complete OB media. Cells were incubated in standard growth media for 7 or 14 days, with media replaced every 3 days.[30,36]

2.7 | Osteoblast cell activity

To quantify *in vitro* biological properties, hOB cell activity was monitored at 7 and 14 days using an alamarBlue (Bio-Rad, Hercules, CA, USA) assay. The alamarBlue solution is a resazurin salt solution that changes color based on metabolized proteins released by active cells.[39] A greater change in color from blue to magenta indicates a reduction of alamarBlue and hence the increased presence of live/active cells. The sample size for all composite loadings, npHA, and cell-drop control was $n = 3$ at both 7 and 14 days. Separate samples were monitored at 7 and 14 days to prevent any errors from additional alamarBlue reduction, resulting in 36 samples total. Composite loading samples were randomly selected for the 7 or 14 day timepoint from the six scaffold samples.

At 7 and 14 days, samples were aspirated of media, flushed with $1\times$ PBS, and then aseptically transferred to a new sterile well plate. This well plate contained 5 vol% alamarBlue solution in 2 mL of complete hOB media. Cell-drop controls were aspirated of media, flushed

with $1\times$ PBS, and then filled with 2 mL of 5% alamarBlue hOB media. Next the samples were incubated for 24 h to ensure a measurable change in alamarBlue reduction. In triplicate, 100 μL of the assay media was transferred to a 96-well plate, and fluorescence was measured through a spectrophotometer (SpectraMax M3, Molecular Devices, San Jose, CA, USA) at 560 and 590 nm wavelengths with an incident wavelength of 590 nm. The fluorescence data were subsequently normalized to the npHA control after 7 days of incubation to compare growth rates to a set baseline.[40]

2.8 | Statistical analysis

All data analyses were performed using MATLAB 2021b (MathWorks, Natick, MA, USA). Between-group comparisons were performed using analysis of variance (ANOVA). If data was found to be non-normal through a Shapiro–Wilks test or heteroscedastic through Levene's test (for normal data) or Bartlett's test (for non-normal data), a Kruskal–Wallis test was performed instead as the nonparametric counterpart to the ANOVA. Tukey's honest significant difference (HSD) tests or Dunn's tests were used for pair-wise comparisons given a statistically significant result ($\alpha = .05$) from the ANOVA or Kruskal–Wallis test, respectively. Bonferroni's correction was used to further reduce Type I errors by dividing α by the number of pair-wise comparisons.

3 | RESULTS AND DISCUSSION

### 3.1 | Microstructural characterization

The microstructures of the freeze-cast HA-TiO$_2$ scaffolds perpendicular to the ice growth direction are shown in Figure 1. No significant differences were found between composite loadings for pore size ($p = .518$), porosity ($p = .832$), or wall thickness ($p = .685$), with values shown in Table 2. These properties are reflected in the SEM images as the structures remained consistent between composite loadings. The major and minor axes of the pores are also provided in Table 2. The pore size (as calculated by the equivalent diameter) of $\sim$30 μm matched past records of freeze-cast HA.[41] While the equivalent diameter is used as the main comparison for pore size, the major and minor axes help represent the geometry of the pores. The major axis averaged above 110 μm in all scaffolds with a minor axis of around 16.5 μm, which would allow cells to propagate through the pores.[3,42,43] This microstructure matches previous HA scaffolds made through freeze casting with water.[44–46] While Haugen et al.[3] suggested that the ideal pore size for human bone growth should be at least 100 μm, successful bone growth has been observed in freeze-cast scaffolds with pores less than 100 μm.[47–51] The oriented pore structure gained from freeze casting has also shown potential benefits over an isotropic pore structure.[51,52] In general, the open porosity of these scaffolds would allow for nutrient and waste transportation as well as cell migration and proliferation throughout the scaffold.

3.2 | Material characterization

Electron dispersive x-ray spectroscopy (Figure 2) was performed to understand how the HA and TiO$_2$ particles interacted during the freeze-casting process. Regions of HA and TiO$_2$ were identified by comparing the presence of calcium and titanium, respectively, within observed regions. With increasing TiO$_2$ content, the HA scaffold walls shifted from a substrate with distributed TiO$_2$ particles embedded in it to the distributed HA particles themselves embedded in a TiO$_2$ substrate. Phase segregation was minor, given the even distribution of HA and TiO$_2$ particles through the structure, as seen in all images. This mixing could likely be attributed to the use of ultrasonication[53,54] and the use of the Dynol 604 dispersant[29,41] to ensure particles are properly dispersed. Initial particle sizes before sintering would have caused the larger grains that are present in the scaffold walls. The addition of Dynol 604 as the dispersant also likely played a role to prevent flocculation and phase separation between the HA and TiO$_2$.[29]

Other ceramic–ceramic composites have been made through freeze casting, but these reports lack element distribution analyses within the microstructure. Dong et al. fabricated alumina-mullite composites through freeze casting that successfully mimics the hierarchical structure of bone.[55] Liu and Button have also created alumina-zirconia composites and found that the differences in density and particle size could lead to phase segregation within a mixed slurry.[56] As the particle size and density were relatively similar between HA and TiO$_2$, this may have helped reduce phase segregation during freeze casting. As mentioned earlier, both materials are thermally stable of up to 1250°C, likely leading to a stable composite structure. This stability may not have been observed if materials such as alumina or zirconia, which need sintering above 1400°C, had been mixed with the HA instead of TiO$_2$.[57–59] As such, proper mixing, slurry composition, and thermal stability led to a stable and well-mixed ceramic composite fabrication using the freeze casting process.

Looking at the phase compositions of the composites using XRD (Figure 3), all composites showed high crystallinity indicated by the multiple sharp peaks, but differences in intensity were observed between the different HA-TiO$_2$ sintered composites. Compared to HA with a peak at the 30° angle, peaks have shifted to the 35° angle in composite loading samples, indicating new phase development in the samples likely to be in the forms of β-tricalcium phosphate (β-TCP) [Ca$_3$(PO$_4$)$_2$] and calcium titanate [CaTiO$_3$]. These shifts were interpreted as the reaction that occurs at the interfaces between HA and TiO$_2$ as the transformation of HA into β-TCP and the formation of CaTiO$_3$ as shown in (1).[60,61]

$$Ca_{10}(PO_4)_6(OH)_2 + TiO_2 \rightarrow 3Ca_3(PO_4)_2 + CaTiO_3 + H_2O \quad (1)$$
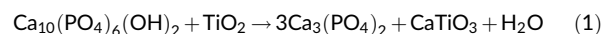
Other potential phases may have been present, but their peaks may have been hidden by the more prevalent phases, especially with increasing TiO$_2$ content. Sintering above 1300°C is known to cause HA to change into β-TCP.[37,62,63] While the HA scaffolds did not undergo this phase change when sintering at 1250°C, the presence of TiO$_2$ perhaps helped catalyze the reaction at a lower temperature in the composite scaffolds through dehydration which explains the

FIGURE 1 SEM images of microstructure at lower and higher magnifications for HA (A, B), HT-25 (C, D), HT-50 (E, F), and HT-75 (G, H).
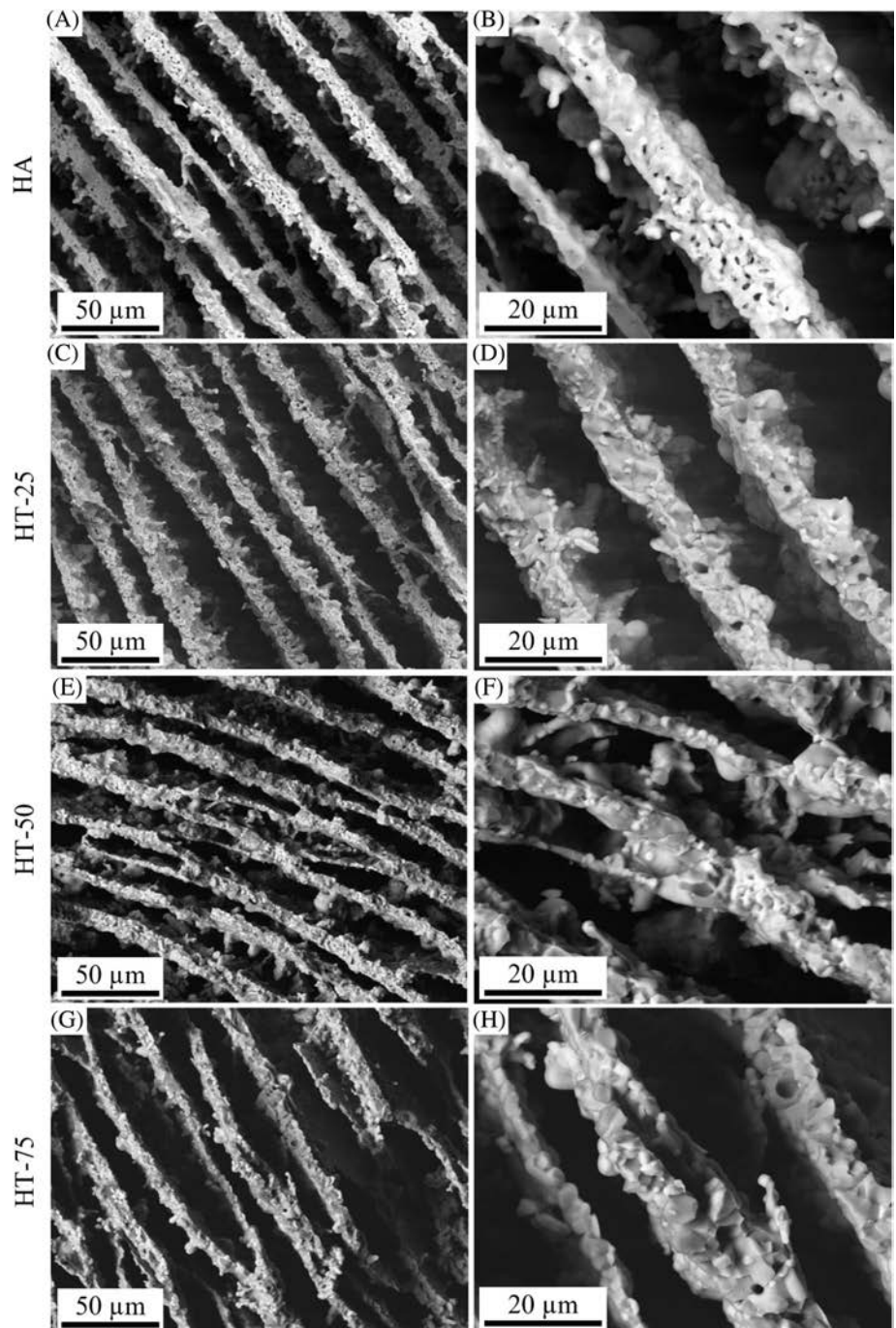
transformation of HA into β-TCP.[60] This data agrees with past XRD data on HA-TiO$_2$ composites from Lee et al.[64] and Nath et al.[65] found β-TCP, CaTiO$_3$, and rutile TiO$_2$ phases, which are also present in our composite loading samples. The presence of β-TCP can be beneficial for bone substitutes due to its higher biodegradability despite its lower mechanical strength than HA.[9,11,15] CaTiO$_3$ has also been reported to improve biocompatibility and osseointegration when used as a coating on titanium implants.[66,67] Even though most of the HA has been transformed into β-TCP and CaTiO$_3$ has been observed, HA will continue to be used for simplicity.

While the presented data has been normalized, the peak intensities were observed to have decreased with increasing TiO$_2$,

suggesting a higher crystallinity compared to HA. These results are similar to those found by Khattab et al.,[68] who fabricated HA-TiO$_2$ composites using freeze gel casting and starch consolidation. They noted that lower peaks in the composite samples indicate the presence of calcium phosphate either in the form of HA or other phases such as, β-TCP, which may have occurred due to sintering. Through the EDX and XRD data, it can be determined that the sintering of HA-TiO$_2$ at 1250°C provided a well-mixed and stable composite structure. In future studies, it is worth investigating the XRD data for differing sintering temperatures on freeze-cast HA-TiO$_2$ composites to understand the role of temperature in the β-TCP phase transformation.

Property	HA	HT-25	HT-50	HT-75
Porosity (%)	55.2 ± 11.0	53.0 ± 7.1	54.0 ± 6.5	52.7 ± 6.6
Equivalent diameter (μm)	30.5 ± 13.4	30.9 ± 12.0	31.8 ± 13.4	31.4 ± 14.3
Wall thickness (μm)	10.8 ± 2.7	9.8 ± 2.3	10.7 ± 3.0	10.7 ± 2.3
Major axis (μm)	113 ± 72.7	117 ± 73.1	119 ± 78.5	118 ± 80.4
Minor axis (μm)	16.7 ± 10.0	16.4 ± 6.9	16.6 ± 6.7	16.7 ± 7.5

TABLE 2 Microstructural properties by composite loading.

Note: Data is displayed as mean ± standard deviation. For porosity: $n = 15$ per composite loading. For all other properties: $n = 1200$ per composite loading.
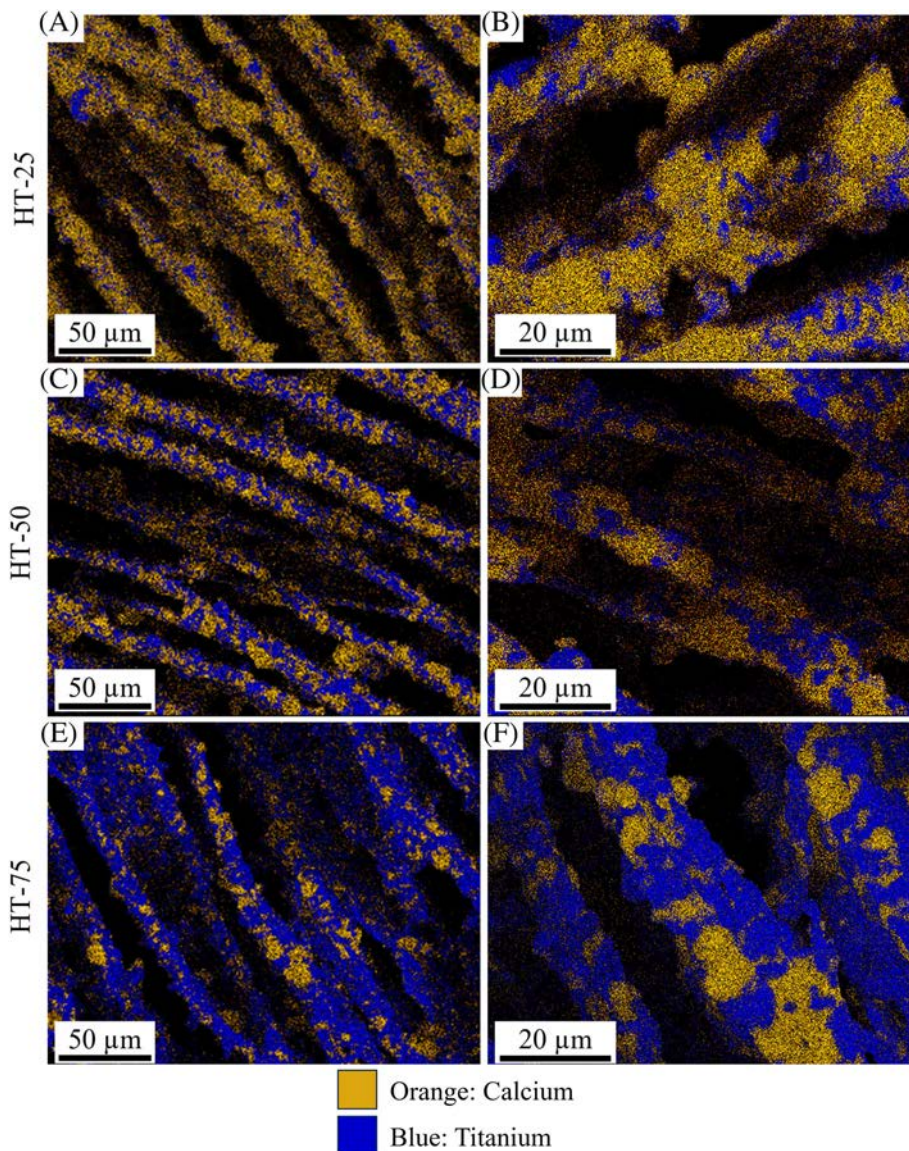

FIGURE 2 EDX images at lower and higher magnifications for HT-25 (A, B), HT-50, (C, D), and HT-75 (E, F). Calcium is shown in orange. Titanium is shown in blue.

3.3 | Mechanical response

Figure 4 shows the results for UCS and E for each composite loading ($n = 11$ per composite loading). All composite ultimate compressive strengths were greater than the HA UCS (1.57 ± 0.37 MPa) with statistical significance ($p < .006$). HT-50 showed the greatest UCS of 3.12 ± 0.36 MPa with a significant difference from HT-75 with a UCS of 2.32 ± 0.67 MPa ($p = .017$), but no significant differences were observed in UCS when compared to HT-25 with a UCS of 2.79 ± 0.58 ($p = .734$). No significant difference was observed between HT-25 and HT-75 UCS as well ($p = .171$). The stiffness also increased by adding TiO_2 when compared to only HA. HT-25 with an E of 62.63 ± 21.33 MPa and HT-50 with an E of 63.29 ± 28.75 had a stiffness greater than that of HA with E 32.49 ± 14.36 ($p < .001$).

However, no significant difference was found between stiffness for HT-75 with an E of 49.45 ± 19.10 and HA ($p = .541$). The composite ultimate compressive strengths are comparable to the trabecular bone where UCS is 2–12 MPa, while the elastic moduli are just below the lower limit of trabecular bone (0.1–5 GPa).[69]

From sintering at 1250°C, the composite loadings showed greater strength and stiffness when compared to HA. Because pore size remained the same, the increase in mechanical properties can most likely be attributed to the addition of TiO$_2$ due to its greater strength compared to HA.[9,10,70,71] Ho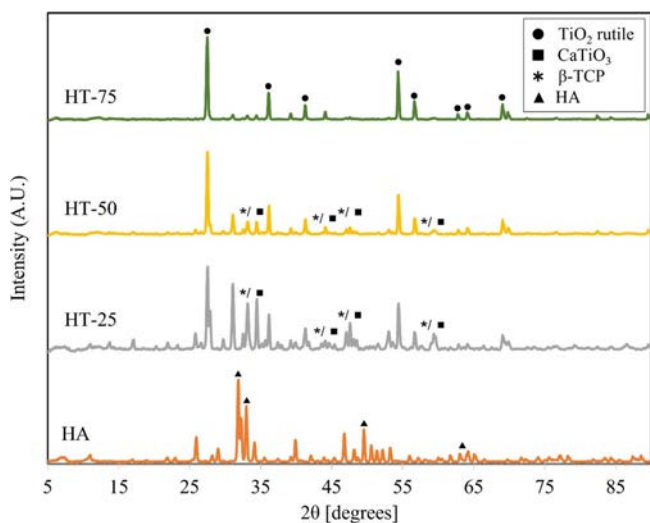wever, it is interesting to note that the properties did not increase linearly with increasing TiO$_2$ content, instead reaching the highest observed strength in HT-50 samples. We believe that there are a few interconnected factors that have influenced these mechanical properties of the composite loadings—namely doping, interfacial bonding, and grain/crystal size. Doping of weaker materials like HA with stronger materials like TiO$_2$ and other ceramics or metals has been shown to improve the mechanical strength of HA.[72–75] This doping effect for increased mechanical properties was observed in all composite loadings since they had greater mechanical properties than HA.

As observed through XRD, the HA in the composite loading samples had mostly been transformed into β-TCP which by itself is weaker compared to HA.[9,15,76] However, by also providing strong interfacial bonding through phases like CaTiO$_3$, toughness and strength could increase due to greater crack deflection and energy absorption at the Ca-Ti interfaces.[60,77] Composite HA-TiO$_2$ porous scaffolds made through direct foaming method resulted in a UCS and E within the range of trabecular bone.[60] Similarly, Sprio et al.[24] observed increases in flexural strength and fracture toughness in non-porous HA samples containing up to 30% TiO$_2$ sintered at 1250°C when compared to just HA. The current results further our understanding of improving the mechanical properties with up to 50% TiO$_2$ added to HA.

It is widely known that larger grain sizes lead to weaker materials because a crack can propagate through a single grain more easily than if it is deflected at a grain boundary.[78] The grain size of rutile TiO$_2$ has been found to increase with sintering temperature from 500 to 900°C, which would also mean further grain growth at higher sintering temperatures like that used in this study (1250°C).[79,80] For HA which is naturally brittle,[10,81] doping is often used to mitigate this less desirable trait.[75] Doping of TiO$_2$ with calcium and strontium ions was also reported to both reduce grain size and provide interfacial bonding

FIGURE 3 XRD spectra of HA, HT-25, HT-50, and HT-75. HA markers (▲) from ICDD-01-080-6199. β-TCP markers (∗) from ICDD-01-086-1585. CaTiO$_3$ markers (■) from ICDD-01-079-5792. TiO$_2$ rutile markers (●) from ICDD-01-094-1284. $n = 4$ per composite loading.
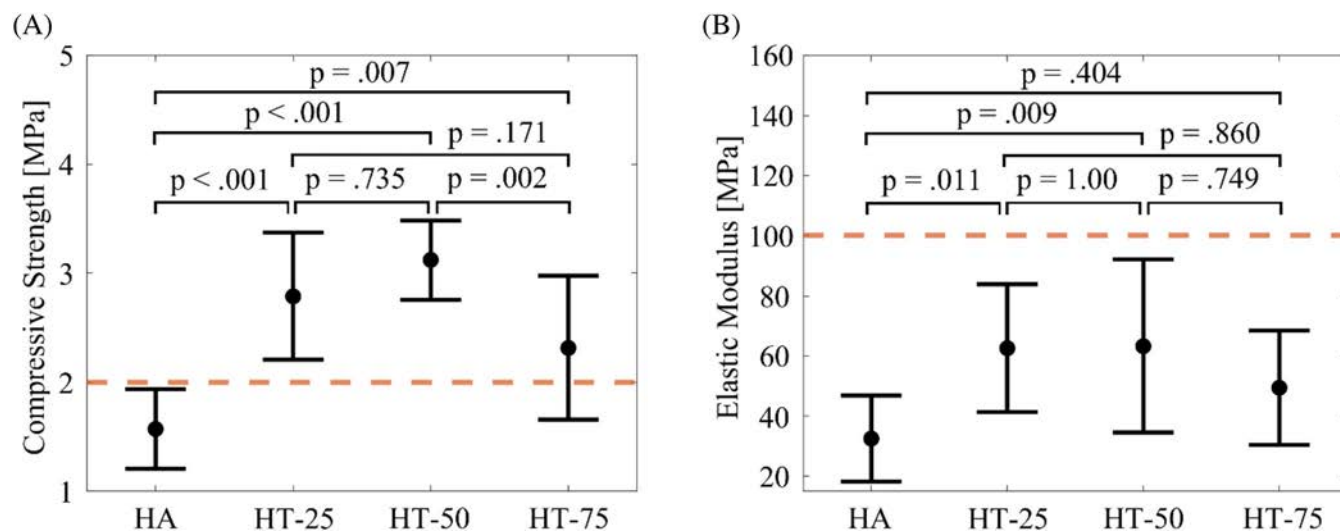

FIGURE 4 UCS (A) and E (B) by composite loading. Data is displayed as the mean ± standard deviation of $n = 11$ per composite loading. Statistical significance ($p < .05$) between groups is noted by p-values above brackets corresponding to pairwise comparisons. Trabecular bone lower limits for UCS (2 MPa) and E (0.1 GPa) are shown as dashed lines.[64]

at grain boundaries which increased mechanical strength.[82,83] Through the combined HA and TiO_2 solid loading, smaller grain size and the presence of interfacial bonding are occurring in the composite scaffolds. Combined with the EDX analysis which showed more evenly distributed regions of calcium and titanium in HT-50 samples, lower mechanical properties in HT-25 and HT-75 were thus attributed to larger grain sizes[79,80,82] from sintering and fewer interfacial boundaries[83,84] from the composite loading as previously reported. In contrast, the better balance of HA and TiO_2 in HT-50 led to a more optimal combination of the factors that resulted in stronger scaffold when sintered at 1250°C.[82–84]

As suggested, the TiO_2 content therefore increased the UCS and E compared to HA alone and reached an experimental maximum in HT-50 with a UCS of 3.12 ± 0.36 MPa and an E of 63.29 ± 28.75 MPa. These HA-TiO_2 composite scaffolds showed greater mechanical properties compared to HA scaffolds, possibly related to a combination of interconnected factors of doping, interfacial bonding, and grain size. Notably, sintering temperature may have also caused larger grains to form, and, while outside the scope of this research, different sintering parameters could cause different properties. These properties need further focus in future studies.

3.4 | Osteoblast cell activity

In vitro hOB cell activity measured through alamarBlue assay is shown in Figure 5. The measured fluorescence intensities were normalized to the intensity of npHA scaffolds after 7 days of culturing to compare cell proliferation a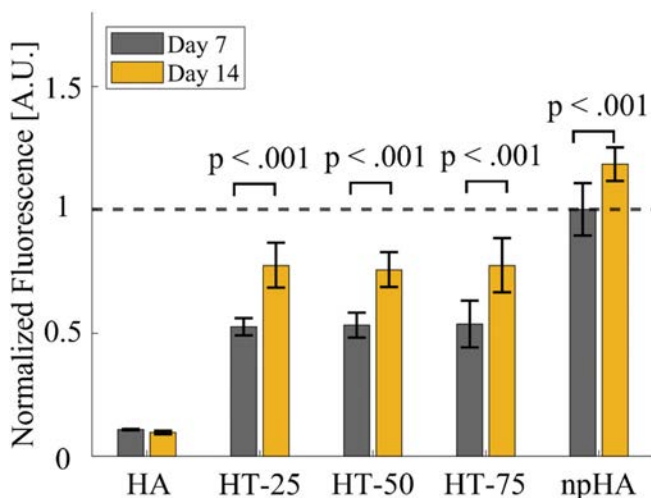fter 7 and 14 days more easily. Cell-drop controls are not shown as they showed much greater cell activity in comparison to the scaffold samples. Composite scaffolds had lower cell activity during the experiment compared to npHA samples. However, the composite scaffolds showed greater relative cell growth from 7 to 14 days with mean ± standard deviation normalized intensity differences of 0.25 ± 0.10 for HT-25, 0.22 ± 0.09 for HT-50, and 0.24 ± 0.14 for HT-75. In comparison, the intensity change from 7 to 14 days for the npHA was only 0.18 ± 0.13. These changes indicate up to a 50% relative increase in cell growth between 7 and 14 days for composite loadings compared to the 10% relative increase in npHA.

Cell activity was found to increase on composite loading scaffolds when compared to porous HA scaffolds. Little to no cell activity was observed on porous HA scaffolds cultured for 7 and 14 days. These results are similar to those reported by Sprio et al.[24] and Cunha et al.,[25] where greater cell activity up to 14 days was also observed on calcium phosphate-titania composites compared to an HA control. These studies noted the importance of this increased cell activity as an important aspect of their materials as potential bone substitutes. Despite the similar microstructure, this limited cell activity indicated poor cell attachment or potentially cell differentiation on the HA scaffolds.[85,86] Im et al.[87] reported increased surface roughness through TiO_2 addition on HA, which positively correlated with increased cell adhesion. Surface roughness on biocompatible materials has been reported to affect cell adhesion, proliferation, and differentiation.[82,88] Given the lower mechanical properties of HA, the HA-TiO_2 composites offered a better substrate to which cells could attach and proliferate while providing the necessary structural strength for load-bearing clinical application.

4 | CONCLUSIONS

In summary, porous HA-TiO_2 scaffolds made through freeze casting were fabricated and characterized. From the results, HA-TiO_2 composites show potential as bone substitutes with appropriate structural, mechanical, and biological properties. Structural analysis indicated similarities in macrostructure to porous HA freeze-cast scaffolds made in the current and past studies.[44–46] Elemental analysis through EDS and XRD showed mixing of the HA and TiO_2 phases during freeze casting, with new phases of β-TCP and $CaTiO_3$ emerging during sintering. This mixing and phase transformation influenced the resultant mechanical properties through doping, interfacial bonding, and crystal size. These composite loading scaffolds increased the mechanical strength and stiffness of the scaffold to the reported range of trabecular bone, and greater than that of the strength and stiffness observed in the HA scaffolds. Lastly, hOB cells proliferated better on composite loading scaffolds and showed increased cell growth when compared to porous HA after 7 days, with further growth in composite loading scaffolds observed at 14 days.

Past research on HA-TiO_2 has largely focused on the physical and biological properties of the composite as a coating for an implant.[66,87,89] Here, we have successfully fabricated porous HA-TiO_2 scaffolds through freeze casting and achieved improved mechanical

FIGURE 5 Cell activity measured through alamarBlue fluorescence at 7 and 14 days for HA, HT-25, HT-50, HT-75, and npHA. Data are normalized to 7-day fluorescence of npHA. Statistical significance ($p < .05$) between 7 and 14 days is noted by p-values above brackets corresponding to pairwise comparisons. All composite loadings' fluorescences are statistically significantly different from npHA fluorescence. Sample size for all composite loadings, npHA, and cell-drop control was $n = 3$ at both 7 and 14 days.

WILEY |

properties and greater *in vitro* cell activity compared to porous HA scaffolds. Thus, freeze casting is a valuable tool in creating simple and cost-effective porous scaffolds, but the possibilities to create HA-TiO$_2$ composites can also extend to other manufacturing techniques like additive manufacturing and gel casting. Future research may also lead to a better understanding of how the composites interact at different sintering temperatures or structural orientations. Studies on mechanical properties and surface roughness in a porous composite scaffold with varying composition may prove especially useful in understanding the subsequent biological attributes of the scaffolds. While doping HA and bioactive glass composites have been studied before, ceramic composites with HA as a substrate still require more attention. Composites offer one solution to improving the flaws of HA and calcium phosphates and can bring current bone substitute options closer to natural bone.

DATA AVAILABILITY STATEMENT

The data that support the findings of this study are available from the corresponding author upon reasonable request.

ORCID

Steven E. Naleway https://orcid.org/0000-0001-9413-0399

REFERENCES

1. Huzum B, Puha B, Necoara RM, et al. Biocompatibility assessment of biomaterials used in orthopedic devices: an overview (Review). *Exp Ther Med*. 2021;22:1-9. doi:10.3892/etm.2021.10750
2. Greenwald AS, Boden SD, Goldberg VM, et al. The committee on biological implants, bone-graft substitutes: facts, fictions, and applications. *J Bone Joint Surg Am*. 2001;83-A(Suppl 2):98-103. doi:10.2106/00004623-200100022-00007
3. Haugen HJ, Lyngstadaas SP, Rossi F, Perale G. Bone grafts: which is the ideal biomaterial? *J Clin Periodontol*. 2019;46:92-102. doi:10.1111/jcpe.13058
4. Baldwin P, Li DJ, Auston DA, Mir HS, Yoon RS, Koval KJ. Autograft, allograft, and bone graft substitutes: clinical evidence and indications for use in the setting of orthopaedic trauma surgery. *J Orthop Trauma*. 2019;33:203-213. doi:10.1097/BOT.0000000000001420
5. Ebrahimi M. Bone grafting substitutes in dentistry: general criteria for proper selection and successful application. *IOSR J Dent Med Sci*. 2017;16(4):75-79.
6. Hasan A, Byambaa B, Morshed M, et al. Advances in osteobiologic materials for bone substitutes. *J Tissue Eng Regen Med*. 2018;12:1448-1468. doi:10.1002/term.2677
7. Zhao R, Yang R, Cooper PR, Khurshid Z, Shavandi A, Ratnayake J. Bone grafts and substitutes in dentistry: a review of current trends and developments. *Molecules*. 2021;26:3007. doi:10.3390/molecules26103007

8. Bhatt RA, Rozental TD. Bone graft substitutes. *Hand Clin*. 2012;28:457-468. doi:10.1016/j.hcl.2012.08.001
9. Yin TJ, Naleway SE. Freeze casting with bioceramics for bone graft substitutes. *Biomed Mater Devices*. 2022. doi:10.1007/s44174-022-00008-1
10. Ginebra M-P, Espanol M, Maazouz Y, Bergez V, Pastorino D. Bioceramics and bone healing. *EFORT Open Rev*. 2018;3:173-183. doi:10.1302/2058-5241.3.170056
11. Fernandez de Grado G, Keller L, Idoux-Gillet Y, et al. Bone substitutes: a review of their characteristics, clinical use, and perspectives for large bone defects management. *J Tissue Eng*. 2018;9:2041731418776819. doi:10.1177/2041731418776819
12. Canillas M, Pena P, de Aza AH, Rodríguez MA. Calcium phosphates for biomedical applications. *Bol Soc Esp Cerám Vidr*. 2017;56:91-112. doi:10.1016/j.bsecv.2017.05.001
13. Ambard AJ, Mueninghoff L. Calcium phosphate cement: review of mechanical and biological properties. *J Prosthodont*. 2006;15:321-328. doi:10.1111/j.1532-849X.2006.00129.x
14. Dehghanghadikolaei A, Fotovvati B. Coating techniques for functional enhancement of metal implants for bone replacement: a review. *Materials*. 2019;12:1795. doi:10.3390/ma12111795
15. Funayama T, Noguchi H, Kumagai H, Sato K, Yoshioka T, Yamazaki M. Unidirectional porous beta-tricalcium phosphate and hydroxyapatite artificial bone: a review of experimental evaluations and clinical applications. *J Artif Organs*. 2021;24:103-110. doi:10.1007/s10047-021-01270-8
16. Nuss KMR, von Rechenberg B. Biocompatibility issues with modern implants in bone – a review for clinical orthopedics. *Open Orthop J*. 2008;2:66-78. doi:10.2174/1874325000802010066
17. Abou Neel EA, Chrzanowski W, Knowles JC. Biological performance of titania containing phosphate-based glasses for bone tissue engineering applications. *Mater Sci Eng C*. 2014;35:307-313. doi:10.1016/j.msec.2013.10.029
18. Dutta SR, Passi D, Singh P, Bhuibhar A. Ceramic and non-ceramic hydroxyapatite as a bone graft material: a brief review. *Ir J Med Sci*. 2015;184:101-106. doi:10.1007/s11845-014-1199-8
19. Kasuga T, Kondo H, Nogami M. Apatite formation on TiO$_2$ in simulated body fluid. *J Cryst Growth*. 2002;235:235-240. doi:10.1016/S0022-0248(01)01782-1
20. Aviles T, Hsu S-M, Clark A, et al. Hydroxyapatite formation on coated titanium implants submerged in simulated body fluid. *Materials*. 2020;13:5593. doi:10.3390/ma13245593
21. Kim H-W, Koh Y-H, Li L-H, Lee S, Kim H-E. Hydroxyapatite coating on titanium substrate with titania buffer layer processed by sol–gel method. *Biomaterials*. 2004;25:2533-2538. doi:10.1016/j.biomaterials.2003.09.041
22. Swapna YV, Mathew CT, Thomas JK. Resistive coupled microwave sintering of hydroxyapatite/titania nano-biocomposite and tailoring its mechanical properties. *J Mech Behav Biomed Mater*. 2023;141:105772. doi:10.1016/j.jmbbm.2023.105772
23. Yao H-L, Yang C, Yang Q, et al. Structure, mechanical and bioactive properties of nanostructured hydroxyapatite/titania composites prepared by microwave sintering. *Mater Chem Phys*. 2020;241:122340. doi:10.1016/j.matchemphys.2019.122340
24. Sprio S, Guicciardi S, Dapporto M, Melandri C, Tampieri A. Synthesis and mechanical behavior of β-tricalcium phosphate/titania composites addressed to regeneration of long bone segments. *J Mech Behav Biomed Mater*. 2013;17:1-10. doi:10.1016/j.jmbbm.2012.07.013
25. Cunha C, Sprio S, Panseri S, Dapporto M, Marcacci M, Tampieri A. High biocompatibility and improved osteogenic potential of novel Ca–P/titania composite scaffolds designed for regeneration of load-bearing segmental bone defects. *J Biomed Mater Res A*. 2013;101A:1612-1619. doi:10.1002/jbm.a.34479

26. Nelson I, Naleway SE. Intrinsic and extrinsic control of freeze casting. *J Mater Res Technol*. 2019;8:2372-2385. doi:10.1016/j.jmrt.2018.11.011

27. Deville S. Ice-templating, freeze casting: beyond materials processing. *J Mater Res*. 2013;28:2202-2219. doi:10.1557/jmr.2013.105

28. Deville S. Freeze-casting of porous biomaterials: structure, properties and opportunities. *Materials*. 2010;3:1913-1927. doi:10.3390/ma3031913

29. Fu Q, Rahaman MN, Dogan F, Bal BS. Freeze casting of porous hydroxyapatite scaffolds. I. Processing and general microstructure. *J Biomed Mater Res B Appl Biomater*. 2008;86B:125-135. doi:10.1002/jbm.b.30997

30. Yin TJ, Jeyapalina S, Naleway SE. Characterization of porous fluoro-hydroxyapatite bone-scaffolds fabricated using freeze casting. *J Mech Behav Biomed Mater*. 2021;123:104717. doi:10.1016/j.jmbbm.2021.104717

31. Naleway SE, Yu CF, Hsiong RL, et al. Bioinspired intrinsic control of freeze cast composites: harnessing hydrophobic hydration and clathrate hydrates. *Acta Mater*. 2016;114:67-79. doi:10.1016/j.actamat.2016.05.019

32. Nelson I, Varga J, Wadsworth P, et al. Helical and Bouligand porous scaffolds fabricated by dynamic low strength magnetic field freeze casting. *JOM*. 2020;72:1498-1508. doi:10.1007/s11837-019-04002-9

33. Silva AMA, Nunes EHM, Souza DF, et al. Effect of titania addition on the properties of freeze-cast alumina samples. *Ceram Int*. 2015;41:10467-10475. doi:10.1016/j.ceramint.2015.04.132

34. Nelson I, Gardner L, Carlson K, Naleway SE. Freeze casting of iron oxide subject to a tri-axial nested Helmholtz-coils driven uniform magnetic field for tailored porous scaffolds. *Acta Mater*. 2019;173:106-116. doi:10.1016/j.actamat.2019.05.003

35. Souza DF, Nunes EHM, Pimenta DS, et al. Synthesis and structural evaluation of freeze-cast porous alumina. *Mater Char*. 2014;96:183-195. doi:10.1016/j.matchar.2014.08.009

36. Bennett BT, Beck JP, Papangkorn K, et al. Characterization and evaluation of fluoridated apatites for the development of infection-free percutaneous devices. *Mater Sci Eng C Mater Biol Appl*. 2019;100:665-675. doi:10.1016/j.msec.2019.03.025

37. Deville S, Saiz E, Tomsia AP. Freeze casting of hydroxyapatite scaffolds for bone tissue engineering. *Biomaterials*. 2006;27:5480-5489. doi:10.1016/j.biomaterials.2006.06.028

38. Hotaling NA, Bharti K, Kriel H, Simon CG. DiameterJ: a validated open source nanofiber diameter measurement tool. *Biomaterials*. 2015;61:327-338. doi:10.1016/j.biomaterials.2015.05.015

39. O'Brien J, Wilson I, Orton T, Pognan F. Investigation of the Alamar blue (resazurin) fluorescent dye for the assessment of mammalian cell cytotoxicity. *Eur J Biochem*. 2000;267:5421-5426. doi:10.1046/j.1432-1327.2000.01606.x

40. Jung J-Y, Naleway SE, Maker YN, et al. 3D printed templating of extrinsic freeze-casting for macro–microporous biomaterials. *ACS Biomater Sci Eng*. 2019;5:2122-2133. doi:10.1021/acsbiomaterials.8b01308

41. Scotti KL, Dunand DC. Freeze casting – a review of processing, microstructure and properties via the open data repository, FreezeCasting.net. *Prog Mater Sci*. 2018;94:243-305. doi:10.1016/j.pmatsci.2018.01.001

42. Iviglia G, Kargozar S, Baino F. Biomaterials, current strategies, and novel nano-technological approaches for periodontal regeneration. *J Funct Biomater*. 2019;10:3. doi:10.3390/jfb10010003

43. Abbasi N, Hamlet S, Love RM, Nguyen N-T. Porous scaffolds for bone regeneration. *J Sci Adv Mater Devices*. 2020;5:1-9. doi:10.1016/j.jsamd.2020.01.007

44. Zamanian A, Farhangdoust S, Yasaei M, Khorami M, Hafezi M. The effect of particle size on the mechanical and microstructural properties of freeze-casted macroporous hydroxyapatite scaffolds. *Int J Appl Ceram Technol*. 2014;11:12-21. doi:10.1111/ijac.12031

45. Cheng Z, Yang YC, Wu ZP. Controlling the structure of hydroxyapatite ceramics with dual pores prepared using freeze-casting. *J Nanotechnol*. 2018;2018:e7531464. doi:10.1155/2018/7531464

46. Jia Z-Q, Guo Z-X, Chen F, Li J-J, Zhao L, Zhang L. Microstructure, phase compositions and in vitro evaluation of freeze casting hydroxyapatite-silica scaffolds. *Ceram Int*. 2018;44:3636-3643. doi:10.1016/j.ceramint.2017.11.114

47. Fisher JP, Vehof JWM, Dean D, et al. Soft and hard tissue response to photocrosslinked poly(propylene fumarate) scaffolds in a rabbit model. *J Biomed Mater Res*. 2002;59:547-556. doi:10.1002/jbm.1268

48. Roy TD, Simon JL, Ricci JL, Rekow ED, Thompson VP, Parsons JR. Performance of degradable composite bone repair products made via three-dimensional fabrication techniques. *J Biomed Mater Res A*. 2003;66:283-291. doi:10.1002/jbm.a.10582

49. Tsuruga E, Takita H, Itoh H, Wakisaka Y, Kuboki Y. Pore size of porous hydroxyapatite as the cell-substratum controls BMP-induced osteogenesis. *J Biochem (Tokyo)*. 1997;121:317-324. doi:10.1093/oxfordjournals.jbchem.a021589

50. Akay G, Birch MA, Bokhari MA. Microcellular polyHIPE polymer supports osteoblast growth and bone formation in vitro. *Biomaterials*. 2004;25:3991-4000. doi:10.1016/j.biomaterials.2003.10.086

51. Liu X, Rahaman MN, Fu Q. Bone regeneration in strong porous bioactive glass (13–93) scaffolds with an oriented microstructure implanted in rat calvarial defects. *Acta Biomater*. 2013;9:4889-4898. doi:10.1016/j.actbio.2012.08.029

52. Fu Q, Rahaman MN, Bal BS, Kuroki K, Brown RF. In vivo evaluation of 13-93 bioactive glass scaffolds with trabecular and oriented microstructures in a subcutaneous rat implantation model. *J Biomed Mater Res A*. 2010;95:235-244. doi:10.1002/jbm.a.32827

53. Milani AS, Radman F, Rahbani B, et al. Effect of different mixing methods on physicochemical properties of mineral trioxide aggregate: a systematic review. *Int J Dent*. 2023;2023:1-15. doi:10.1155/2023/5226095

54. Mahbubul IM, Chong T, Khaleduzzaman SS, et al. Effect of ultrasonication duration on colloidal structure and viscosity of alumina-water nanofluid. *Ind Eng Chem Res*. 2014;53:6677-6684. doi:10.1021/ie500705j

55. Dong X, Chua BW, Li T, Zhai W. Multi-directional freeze casting of porous ceramics with bone-inspired microstructure. *Mater Des*. 2022;224:111344. doi:10.1016/j.matdes.2022.111344

56. Liu G, Button TW. The effect of particle size in freeze casting of porous alumina–zirconia composite. *Ceram Int*. 2013;39:8507-8512. doi:10.1016/j.ceramint.2013.02.101

57. Cutler IB, Bradshaw C, Christensen CJ, Hyatt EP. Sintering of alumina at temperatures of 1400°C and below. *J Am Ceram Soc*. 1957;40:134-139. doi:10.1111/j.1151-2916.1957.tb12589.x

58. Olszyna AR, Marchlewski P, Kurzydłowski KJ. Sintering of high-density, high-purity alumina ceramics. *Ceram Int*. 1997;23:323-328. doi:10.1016/S0272-8842(96)00031-4

59. Stawarczyk B, Ozcan M, Hallmann L, Ender A, Mehl A, Hämmerlet CHF. The effect of zirconia sintering temperature on flexural strength, grain size, and contrast ratio. *Clin Oral Investig*. 2013;17:269-274. doi:10.1007/s00784-012-0692-6

60. Dapporto M, Tampieri A, Sprio S, Dapporto M, Tampieri A, Sprio S. Composite calcium phosphate/titania scaffolds in bone tissue engineering. *Appl Titan Dioxide*. IntechOpen; 2017. doi:10.5772/intechopen.68867

61. Que W, Khor KA, Xu JL, Yu LG. Hydroxyapatite/titania nanocomposites derived by combining high-energy ball milling with spark plasma sintering processes. *J Eur Ceram Soc*. 2008;28:3083-3090. doi:10.1016/j.jeurceramsoc.2008.05.016

62. Zamanian A, Farhangdoust S, Yasaei M, Khorami M, Abbasabadi M. The effect of sintering temperature on the microstructural and mechanical characteristics of hydroxyapatite macroporous scaffolds prepared via freeze-casting. *Key Eng Mater*. 2013;529–530:133-137. doi:10.4028/www.scientific.net/KEM.529-530.133

63. Ruys AJ, Wei M, Sorrell CC, Dickson MR, Brandwood A, Milthorpe BK. Sintering effects on the strength of hydroxyapatite. *Biomaterials*. 1995;16:409-415. doi:10.1016/0142-9612(95)98859-C

64. Lee JK, Jung HC, Seo DS, Kim H, Hwang KH. Preparation of β-TCP/TiO$_2$ composite by hot-pressing. *Solid State Phenom*. 2007;121–123:983-986. doi:10.4028/www.scientific.net/SSP.121-123.983

65. Nath S, Tripathi R, Basu B. Understanding phase stability, microstructure development and biocompatibility in calcium phosphate–titania composites, synthesized from hydroxyapatite and titanium powder mix. *Mater Sci Eng C*. 2009;29:97-107. doi:10.1016/j.msec.2008.05.019

66. Hu H, Liu X, Ding C. Preparation and in vitro evaluation of nanostructured TiO$_2$/TCP composite coating by plasma electrolytic oxidation. *J Alloys Compd*. 2010;498:172-178. doi:10.1016/j.jallcom.2010.03.147

67. Sato M, Aslani A, Sambito MA, Kalkhoran NM, Slamovich EB, Webster TJ. Nanocrystalline hydroxyapatite/titania coatings on titanium improves osteoblast adhesion. *J Biomed Mater Res A*. 2008;84A:265-272. doi:10.1002/jbm.a.31469

68. Khattab RM, Badr HA, Zawrah MF. Effect of processing techniques on properties of porous TiO$_2$ and TiO$_2$/hydroxyapatite composites. *Ceram Int*. 2018;44:8643-8649. doi:10.1016/j.ceramint.2018.02.084

69. Fung Y-C. Bone and cartilage. In: Fung Y-C, ed. *Biomech. Mech. Prop. Living Tissues*. Springer; 1993:500-544. doi:10.1007/978-1-4757-2257-4_12

70. Hench LL. Bioceramics. *J Am Ceram Soc*. 1998;81:1705-1728. doi:10.1111/j.1151-2916.1998.tb02540.x

71. Jung S, Kim JH. Sintering characteristics of TiO$_2$ nanoparticles by microwave processing. *Korean J Chem Eng*. 2010;27:645-650. doi:10.1007/s11814-010-0057-2

72. Luo Y, Li D, Zhao J, Yang Z, Kang P. In vivo evaluation of porous lithium-doped hydroxyapatite scaffolds for the treatment of bone defect. *Biomed Mater Eng*. 2018;29:699-721. doi:10.3233/BME-181018

73. Rafique MMA. Hydrothermal processing of phase pure and doped hydroxyapatite and its characterization. *J Encapsul Adsorpt Sci*. 2018;8:720-726. doi:10.4236/jeas.2018.81002

74. Topuz M, Dikici B, Gavgali M, Yilmazer Y. Effect of hydroxyapatite:zirconia volume fraction ratio on mechanical and corrosive properties of Ti-matrix composite scaffolds. *Trans Nonferrous Met Soc China*. 2022;32:882-894. doi:10.1016/S1003-6326(22)65840-0

75. Baskaran T, Mohammad NF, Saleh SSM, Nasir NFM, Daud FDM. Synthesis methods of doped hydroxyapatite: a brief review. *J Phys Conf Ser*. 2021;2071:012008. doi:10.1088/1742-6596/2071/1/012008

76. Ogose A, Hotta T, Kawashima H, et al. Comparison of hydroxyapatite and beta tricalcium phosphate as bone substitutes after excision of bone tumors. *J Biomed Mater Res*. 2005;72B:94-101. doi:10.1002/jbm.b.30136

77. Zalnezhad E, Musharavati F, Chen T, et al. Tribo-mechanical properties evaluation of HA/TiO$_2$/CNT nanocomposite. *Sci Rep*. 2021;11:1867. doi:10.1038/s41598-021-81187-7

78. Yoshida K, Nishiyama N, Shinoda Y, Akatsu T, Wakai F. Evaluation of effects of crack deflection and grain bridging on toughening of nano-crystalline SiO$_2$ stishovite. *J Eur Ceram Soc*. 2017;37:5113-5117. doi:10.1016/j.jeurceramsoc.2017.06.047

79. Tsega Yihunie M. Effect of temperature sintering on grain growth and optical properties of TiO$_2$ nanoparticles. *J Nanomater*. 2023;2023:e3098452. doi:10.1155/2023/3098452

80. Li J, Ye Y, Shen L, Chen J, Zhou H. Densification and grain growth during pressureless sintering of TiO$_2$ nanoceramics. *Mater Sci Eng A*. 2005;390:265-270. doi:10.1016/j.msea.2004.08.025

81. In Y, Amornkitbamrung U, Hong M-H, Shin H. On the crystallization of hydroxyapatite under hydrothermal conditions: role of sebacic acid as an additive. *ACS Omega*. 2020;5:27204-27210. doi:10.1021/acsomega.0c03297

82. Dasgupta S, Tarafder S, Bandyopadhyay A, Bose S. Effect of grain size on mechanical, surface and biological properties of microwave sintered hydroxyapatite. *Mater Sci Eng C*. 2013;33:2846-2854. doi:10.1016/j.msec.2013.03.004

83. Klemm A, Tiainen H. Coagulated concentrated anatase slurry leads to improved strength of ceramic TiO$_2$ bone scaffolds. *Ceram Int*. 2018;44:6265-6271. doi:10.1016/j.ceramint.2018.01.013

84. Klemm A, Tiainen H. Highly porous Sr-doped TiO$_2$ ceramics maintain compressive strength after grain boundary corrosion. *J Eur Ceram Soc*. 2021;41:5721-5727. doi:10.1016/j.jeurceramsoc.2021.04.059

85. Vandamme K, Naert I, Sloten JV, Puers R, Duyck J. Effect of implant surface roughness and loading on Peri-implant bone formation. *J Periodontol*. 2008;79:150-157. doi:10.1902/jop.2008.060413

86. Garg P, Mazur MM, Buck AC, Wandtke ME, Liu J, Ebraheim NA. Prospective review of mesenchymal stem cells differentiation into osteoblasts. *Orthop Surg*. 2017;9:13-19. doi:10.1111/os.12304

87. Im K-H, Kim M-C, Kang D-K, Kim K-N, Kim K-M, Lee Y-K. Hydroxyapatite/titania hybrid coatings on titanium by sol-gel process. *Biomater Res*. 2006;10:224-230.

88. Zhang Y, Chen SE, Shao J, van den Beucken JJJP. Combinatorial surface roughness effects on osteoclastogenesis and osteogenesis. *ACS Appl Mater Interfaces*. 2018;10:36652-36663. doi:10.1021/acsami.8b10992

89. Sidane D, Rammal H, Beljebbar A, et al. Biocompatibility of sol-gel hydroxyapatite-titania composite and bilayer coatings. *Mater Sci Eng C*. 2017;72:650-658. doi:10.1016/j.msec.2016.11.129